Changes in the Young Modulus of hafnium oxide thin films

André Luís Marin Vargas, Fabiana de Araújo Ribeiro, Roberto Hübler *

Physics Faculty, Materials and Nanostructures Laboratory, Pontifical Catholic University of Rio Grande do Sul. Av. Ipiranga 6681, Porto Alegre, RS 90619-900, Brazil

A B S T R A C T

Hafnium-oxide (HfO_2)-based materials have been extensively researched due to their excellent optical and electrical properties. However, the literature data on the mechanical properties of these materials and its preparation for heavy machinery application is very limited. The aim of this work is to deposit hafnium oxide thin films by DC reactive magnetron sputtering with different Young's Modulus from the Ar/O_2 concentration variation in the deposition chamber. The thin films were deposited by DC reactive magnetron sputtering with different Ar/O_2 gas concentrations in plasma. After deposition, HfO_x thin films were characterized through XRD, AFM, RBS and XRF. In this regard, it was observed that the as-deposited HfO_2 films were mostly amorphous in the lower Ar/O_2 gas ratio and transformed to polycrystalline with monoclinic structure as the Ar/O_2 gas ratios grows. RBS technique shows good compromise between the experimental data and the simulated ones. It was possible to tailored the Young Modulus of the films by alter the Ar/O_2 content on the deposition chamber without thermal treatment.

© 2015 Elsevier B.V. All rights reserved.

1. Introduction

Hafnium-oxide (HfO_2)-based materials have been extensively researched due to their excellent optical and electrical properties. They present a high refractive index and high dielectric constant ($k \sim 25$) that makes it an interesting replacement for silicon dioxide in microelectronic applications [1–4]. Intensive efforts have been dedicated to the research of the electrical properties of hafnium oxide thin films. However, the literature data on the mechanical properties of these materials and its preparation for heavy machinery application, even though of critical importance, is very limited [5,6].

The Young Modulus has a major role on the electrical properties and the thermal stability of coatings. It is related to the energy bond between the atoms, where the higher the Young's Modulus is, the greater the atomic bonding energy will be. Thus, the higher the heat capacity and the shear strain resistance are the minor the volume variation of the film will be. Thus, high-temperature coatings are critical technologies for future power-generation systems and industries since the thin film will be stable at elevated temperatures prior to performing the phase transformations [7–9]. On this perspective, tailoring the mechanical properties of the thin films allows to produce a material for any specific application.

Hafnium oxide thin films are produced by several deposition techniques, among which we highlight: RF magnetron sputtering,

atomic layer deposition and CVD. These processes enable rapid and homogeneous deposition of thin films and are widely discussed in review articles [10–12]. On the other hand, DC reactive magnetron sputtering have the ability to produce also nonstoichiometric films with high quality and reproducibility, generating homogeneous coatings with low deposition rate and different oxygen concentration allowing in that way, the deposition of a wide range of structures [13,14]. The aim of this work is to deposit hafnium oxide thin films by DC reactive magnetron sputtering with different Young's Modulus from the Ar/O_2 concentration variation in the deposition chamber.

2. Material and methods

HfO_x thin films were deposited on Si (1 0 0), soda-lime glass and high purity graphite substrates by reactive DC magnetron sputtering technique. The Si (1 0 0) wafers and the soda-lime glass were cleaned in ultrasound during 10 min with isopropyl alcohol, washed with acetone and then washed in DI water. High purity graphite substrates were mirror polished up to grade 4000 sandpaper. A 99.95% pure hafnium target was used as starting material. The vacuum chamber was pumped to a pressure of at least 5×10^{-5} Pa and then filled with a mixture of argon (Ar 6.0) and oxygen (O_2 5.0) until the working pressure of 2×10^{-1} Pa was reached. In the sputtering process the power source (Advanced Energy USA) was maintained constant power of 100 W. The depositions of the films were dynamically controlled by the Ar/O_2

partial pressure ratio using a gas analyzer attached to de vacuum chamber. This system allows to produce oxide coatings with structures from the metal phase to the stoichiometric oxide, as presented on Table 1. Each Ar/O$_2$ condition was deposited on all the substrates in one single process. The Ar and O$_2$ partial pressures were controlled and monitored using a mass gage controller (QMG) inside a differential chamber, which is attached to the main deposition chamber. Detailed information about the deposition equipment can be found at Hübler [15].

HfO$_x$ films deposited on soda-lime glass and Si (1 0 0) were used for X-ray diffraction patterns (GAXRD), X-ray fluorescence (XRF) and instrumented hardness tests (IHT) characterizations. GAXRD was performed by a XRD 7000 Shimadzu equipment, with Bragg – Brentano geometry, applying a Cu Kα radiation (0.15406 nm). The X-ray tube was kept on 3° and 2θ varied between 0° and 40°, always using the sample randomizer (rotating at 60 rpm) in order to standardize the diffraction intensities. IHT were carried out on a Fisherscope HV100 equipment, applying a 5 mN load-unload cycle, during 120 s. IHT were performed according to ISO 14577 regulations. Coatings on graphite were evaluated by Rutherford backscattering spectrometry (RBS) using a Tanden equipment applying an incident alpha particle beam (He++) with energy of 2.0 MeV perpendicular to the samples (θ = 0°) and φ = 15°. Energy calibration was made with Au film with 2.0 MeV energy and an Hf film with 1.5 MeV. RUMP software was used to simulate and to compare theoretical and experimental samples spectra [16]. The morphological analysis was made using Bruker Dimension Icon® Atomic Force Microscope equipment in tapping mode analysis and the images were acquired in a 1 μm area with a 256 × 256 matrix and using a 1 Hz scan rate.

3. Results and discussion

IHT analyses were conducted as soon as the deposited films were removed from the vacuum chamber. Fig. 1 shows the hardness values obtained for each of the deposited coatings. Sample R23 presented the highest hardness value (20 GPa) and sample R2.5 the lowest one (9 GPa). Hardness and Young Modulus presented the same behavior. The values of hardness and elastic modulus presented in the literature vary widely depending on the thermal treatment and mechanical efforts. In general, the reported hardness values are between 1.5 GPa and 22 GPa for the metallic hafnium and from 8.5 GPa to 21 GPa for hafnium oxide, however, these properties have yet to be studied in more detail. The variation of concentration Ar/O$_2$ in the chamber produced thin films with different mechanical properties. Fig. 2 shows the load unload curves for the HfO$_x$ samples where it is possible to observe distinct behaviors for the mechanical response of the films to the load. These regions, however, can be separated into four different ones, due to their diffraction patterns as showed in Fig. 3. Sample R23 presented the characteristic pattern of metallic hafnium hexagonal structures. Sample R17 presented an amorphous structure composed by a mixture of hexagonal metal structure

Table 1
The Ar/O$_2$ partial pressure ratio and film thickness for each samples.

Ar/O$_2$ ratio	Partial pressure (mbar)		Film thickness (nm)
	Ar	O$_2$	
R23	$6.72\cdot10^{-7}$	$2.92\cdot10^{-8}$	2312
R17	$5.57\cdot10^{-7}$	$3.24\cdot10^{-8}$	2248
R10	$8.27\cdot10^{-7}$	$8.07\cdot10^{-1}$	1714
R5	$7.92\cdot10^{-7}$	$1.73\cdot10^{-7}$	612
R2.5	$1.39\cdot10^{-6}$	$5.62\cdot10^{-7}$	328
R0.5	$1.46\cdot10^{-6}$	$2.62\cdot10^{-6}$	374
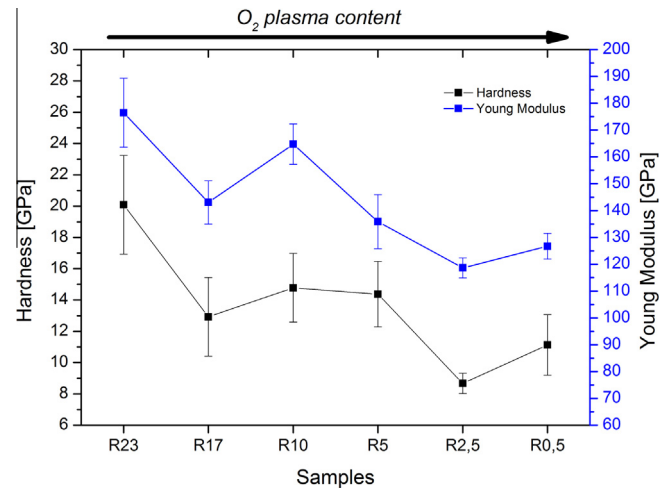
Fig. 1. Hardness and Young's Modulus for which HfO$_x$ thin film as-deposited.
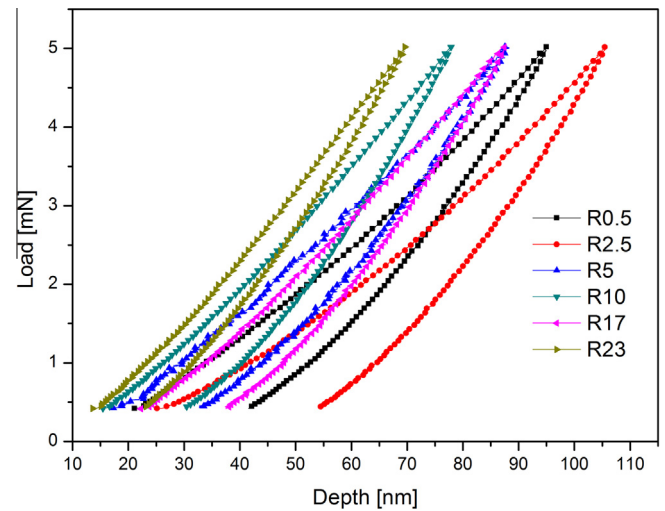
Fig. 2. Typical IHT curve for the deposited HfO$_x$ thin films.
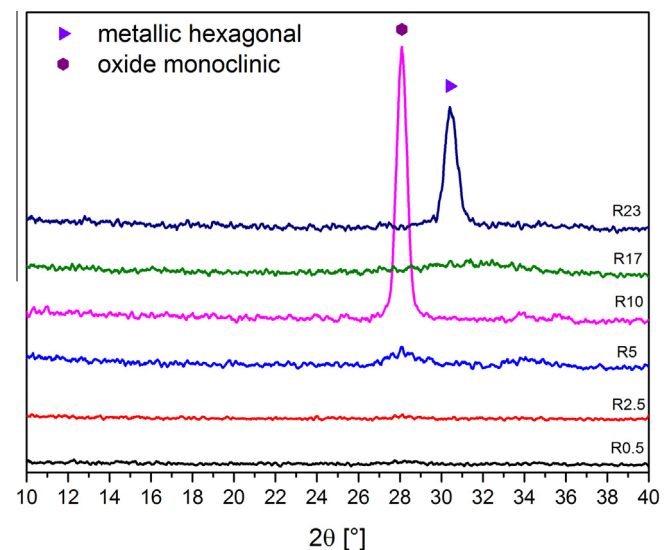
Fig. 3. GAXRD patterns for the HfO$_x$ thin films.

and the monoclinic hafnium oxide structure, indicating a transition region, and the sample R10 shows only a monoclinic structure. In the same way the sample R5 present a lowering of the monoclinic peak, indicating an amorphization of the coating that is reached by samples R2.5 and R0.5. Thus, the results of IHT and XRD corroborate, showing that the results obtained allow the distinction of the samples into four distinct regions, both in mechanical properties and in crystal structures (see Table 2).

This variation in the concentration of gases highlights the data obtained from the XRD and IHT analysis, which allows a better understanding of the four areas listed previously. These regions can be rewritten into five distinct structures: (i) the first one is composed of a metallic phase, which presents metallic hafnium only (R23); (ii) the second one is composed of a mixture of metallic phases and hafnium oxide (R17); (iii) the third one is composed of a monoclinic hafnium structure (R10); (iv) the fourth one is a mixture of the monoclinic structure and the film amorphization (R5) and; (v) an amorphous one (R2.5 and R0.5), entitled A, AB, B, BC and C, respectively, as indicated in Fig. 4.

The chemical composition of the samples was characterized through the XRF technique and the data obtained was used to model the data from the RUMP simulation of the RBS results. The concentrations of oxygen and hafnium measured are showed in Table 3. It is possible to observe that as the oxygen concentration in plasma varies, there is a change in the ratio Hf/O of the deposited films, this variation, however, is not linear. As demonstrated by the analysis of the data in Table 3, the concentrations of oxygen and hafnium were modulated according to the Ar/O$_2$ gas pressure ratios used during the deposition process, forming coatings with different properties, such as: (i) for obtaining coatings with metallic characteristics a high ratio Ar/O$_2$ discharge was used, and the samples were identified by groups A, AB and B; (ii) for the production of thin films with ceramic characteristics a lower ratio of Ar/O$_2$ was used and the samples obtained correspond to the groups BC and C. However, an interesting result was the obtaining of the stoichiometric form of hafnium oxide in sample R0.5.

Fig. 5 shows a typical RBS spectrum for a 390 nm thick film, together with the iteratively adjusted theoretical fit. The O/Hf atomic ratio is less than 2 for all samples in the A, AB and B regions, although it approaches 2 for the lowest Ar/O$_2$ ratio pressure (BC and C regions), which implies that the films contain oxygen-deficient HfO$_{2-x}$. The RBS spectra from the different samples showed a similar behavior, presenting a mixing region on the interface between the carbon substrate and the HfO$_x$ thin film as shown in Fig. 5. Allowing the complete and independent observation of the plateaus for the substrate (C) and film (O and Hf).

The thickness data generated from RUMP simulations enabled the comparison of the deposition rate as a function of oxygen concentration present in each sample Fig. 6. Once acknowledging that the deposition time was kept constant for all samples, it is possible to observe that the deposition rate increases as the ratio Ar/O$_2$ increases (low oxygen pressure). It is well known that the sputtering yield will vary significantly with the concentration of gases in the plasma of a DC magnetron sputtering process. This may occur by the target poisoning and the formation of phases with different
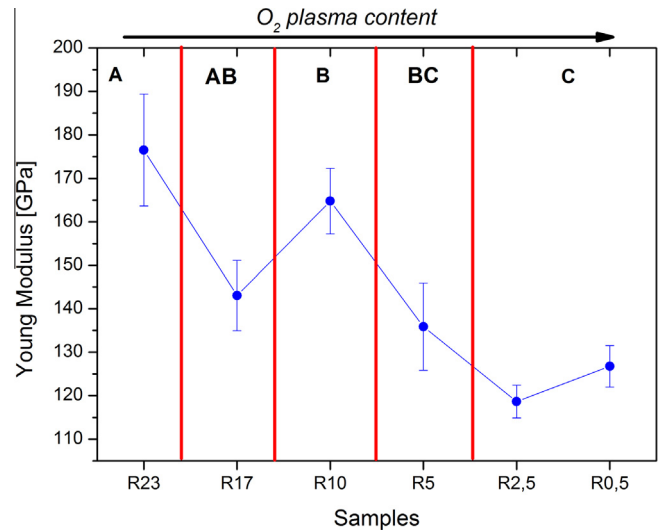
Fig. 4. Young's Modulus rewritten in terms of the GAXRD patterns for the as-deposited hafnium oxide thin films.

Table 3
Composition obtained by XRF, atomic ratio and crystalline region for the HfO$_x$ samples.

Samples	Composition (at.%)		Hf/O ratio	Region
	Ar	O		
R23	11.088	88.912	8.0	A
R17	13.514	86.486	6.4	AB
R10	14.784	85.216	5.0	B
R5	49.374	50.626	1.0	BC
R2.5	74.357	25.643	0.4	C
R0.5	66.500	33.499	0.5	C
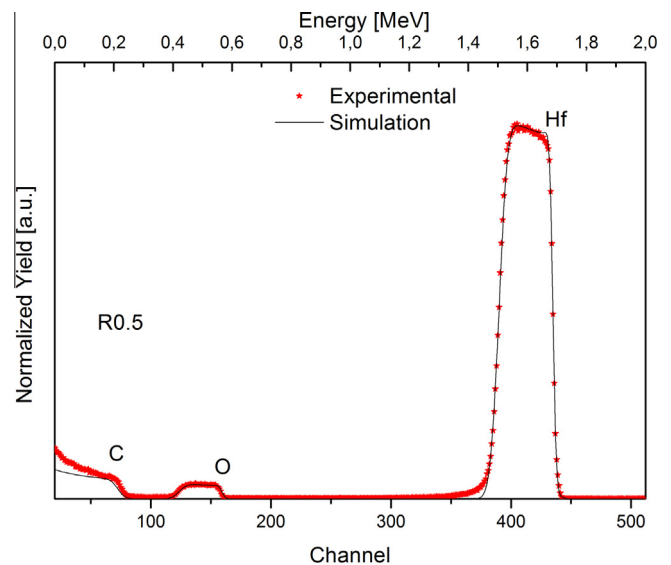
Fig. 5. RBS spectra for sample R0.5 where the stars are the experimental data and the line the RUMP simulation.

binding energies that can facilitate or hinder the removal of the surface atoms. This second option would observe the formation of different phases in the film being deposited as shown in Fig. 6. It is possible to observe in these specific regions an abrupt and significant increases in thickness. Moreover, it is also possible to observe from samples R23 to R17 (regions A and AB on Fig. 6) that

Table 2
Hardness and Young Modulus of the deposited coatings.

Samples	Hardness (GPa)	Young Modulus (GPa)
R23	20.09 ± 3.1	176.51 ± 12.8
R17	12.92 ± 3.5	143.04 ± 18.1
R10	14.78 ± 2.2	164.77 ± 14.5
R5	14.37 ± 4.0	135.89 ± 10.0
R2.5	8.67 ± 0.6	118.65 ± 3.7
R0.5	11.13 ± 1.9	126.74 ± 4.0
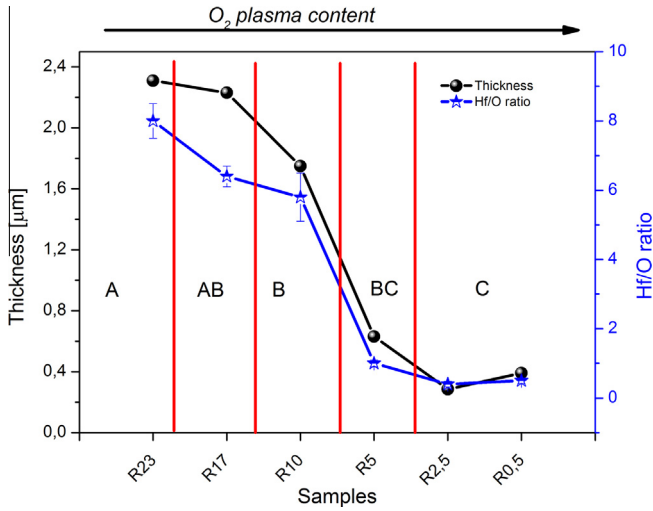
Fig. 6. Thicknesses of the hafnium oxide thin films obtained from the RBS measurements and the relation between the Ar/O_2 ratio concentration and the thickness.

the thickness values remained constant, with no significant interference from variations on oxygen pressure in the chamber, for this band. For samples included in region B a small decrease in thickness occur, however, for ratio R5 (BC region on Fig. 6) a thickness of approximately 0.6 μm was obtained. Presenting the significant difference of approximately 3.5 times compared to samples R23–R10. For samples in region C (R2.5–R0.5 on Fig. 6) the thickness values were very similar (~350 nm) and presented a new decrease when compared to region BC (Fig. 6). These results demonstrate the significance of the influence of oxygen's partial pressures in the rate of HfO$_x$ deposition. Abrupt changes occur only in very specific values of pressure that correspond to bands where there are phase and mechanical property changes. Fact that was expected since changing the structural phase of the film should trigger changes in the binding energies between the constituent elements of it, altering its mechanical properties. These changes all together alter the target's sputtering rate, producing different thickness films, allowing observing the transition regions by any of these techniques. However, when analyzing the oxygen content for each film deposited during the RUMP simulation process we observe a increase on the quantity of this element up to 20% in the deposited samples. This fact has required observation of the morphology of the deposited samples. The AFM images showed a flat surface for all samples as shown by Fig. 7. The sample R23 presented some peak structures on the surface and a roughness Ra of 0.63 nm, this roughness were expected since the amount of metal in the structure promotes flat surfaces (Fig. 7(a)). The sample R10 presented a dendrite type morphological structure and the Ra roughness of 2 nm (Fig. 7(b)). Interestingly, as the Ar/O_2 ratio content decreases in the deposition chamber more flat remained the surface in sample R5 (Ra = 0.22 nm), as shown Fig. 7(c). Unexpected was the roughness for sample R0.5 (Ra = 2.1 nm) that increases in relation to sample R5 even though the amorphous crystalline of these coating indicate similarity with sample R5 (Fig. 7(d)).
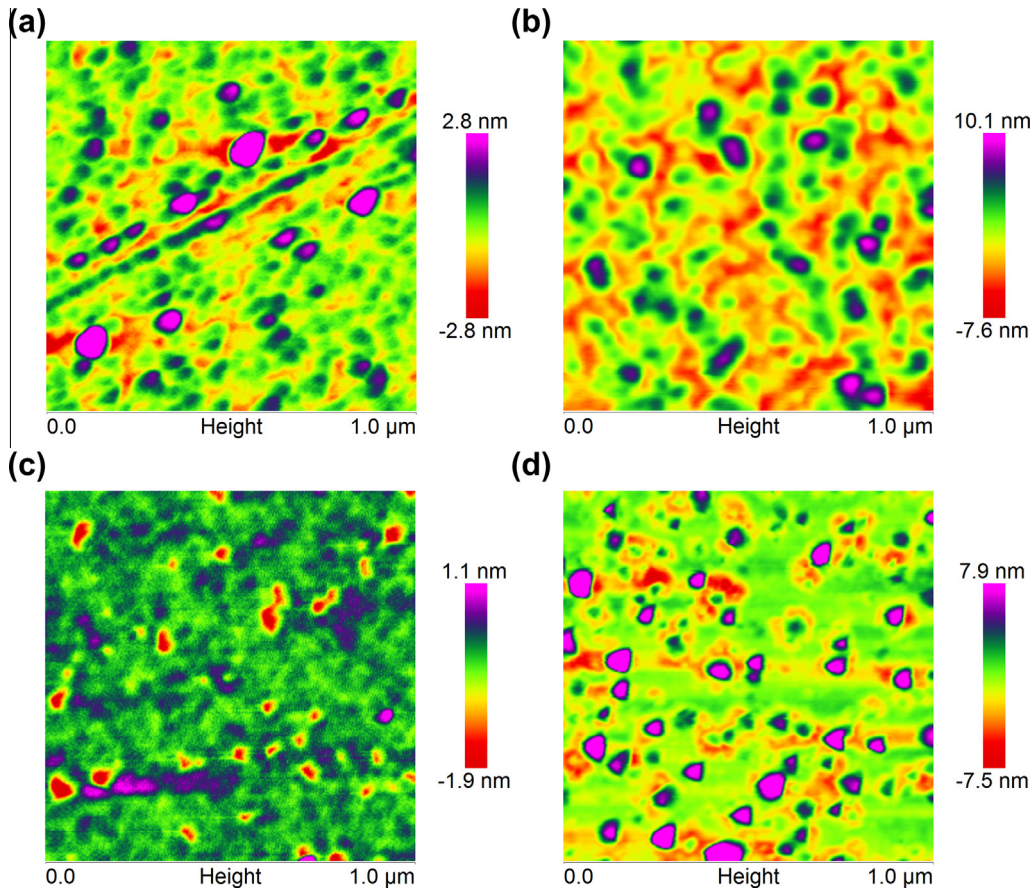
Fig. 7. Surface morphology from the deposited hafnium oxide thin films: (a) R23, (b) R10, (c) R5 and (d) R0.5.

4. Conclusions

Using the DC reactive magnetron sputtering technique it was possible to deposit hafnium oxide thin films with different Young's Modulus. The coatings deposited obtained different oxygen concentration by alter the Ar/O_2 content in the chamber. It was possible observe 5 distinct regions from a metallic phase up to monoclinic phase of hafnium oxide to an amorphous state on the sample R0.5. Interestingly, the R0.5 sample obtained the stoichiometric concentration of hafnium oxide once the sputtering process starts from a metallic target.

Acknowledgments

References

[1] G.D. Wilk, R.M. Wallace, J.M. Anthony, High-κ gate dielectrics: current status and materials properties considerations, J. Appl. Phys. 89 (10) (2001) 5243–5275.

[2] R.K. Nahar, V. Singh, A. Sharma, Study of electrical and microstructure properties of high dielectric hafnium oxide thin film for MOS devices, J. Mater. Sci.: Mater. Electron. 18 (6) (2007) 615–619.

[3] M. Behar et al., Energy loss of proton, particle, and electron beams in hafnium dioxide films, Phys. Rev. A 80 (6) (2009) 062901.

[4] I.Z. Mitrovic et al., Electrical and structural properties of hafnium silicate thin films, Microelectron. Reliab. 47 (4–5) (2007) 645–648.

[5] D.K. Venkatachalam et al., Nanomechanical properties of sputter-deposited HfO_2 and $Hf_xSi_{1-x}O_2$ thin films, J. Appl. Phys. 110 (4) (2011). 043527-5..

[6] W. Zhou et al., Heat capacity of hafnia at low temperature, J. Chem. Thermodyn. 43 (6) (2011) 970–973.

[7] M. Noor-A-Alam, A.R. Choudhuri, C.V. Ramana, Effect of composition on the growth and microstructure of hafnia–zirconia based coatings, Surf. Coat. Technol. 206 (7) (2011) 1628–1633.

[8] M. Hojamberdiev, H.J. Stevens, Indentation recovery of soda-lime silicate glasses containing titania, zirconia and hafnia at low temperatures, Mater. Sci. Eng., A 532 (2012) 456–461.

[9] C.-M. Yang et al., Drift and hysteresis effects improved by RTA treatment on hafnium oxide in pH-sensitive applications, J. Electrochem. Soc. 155 (11) (2008) J326–J330.

[10] J. Robertson, R.M. Wallace, High-K materials and metal gates for CMOS applications, Mater. Sci. Eng., R. 88 (2015) 1–41.

[11] Y. Morita, S. Migita, W. Mizubayashi, M. Masahara, H. Ota, Two-step annealing effects on ultrathin EOT higher-k (k = 40) ALD-HfO$_2$ gate stacks, Solid-State Electron. 84 (2013) 58–64.

[12] J.H. Choi, Y. Mao, J.P. Chang, Development of hafnium based high-k materials—a review, Mater. Sci. Eng. R. 72 (2011) 97–136.

[13] S. Bruns et al., High rate deposition of mixed oxides by controlled reactive magnetron-sputtering from metallic targets, Thin Solid Films 520 (12) (2012) 4122–4126.

[14] O. Stenzel et al., Plasma ion assisted deposition of hafnium dioxide using argon and xenon as process gases, Opt. Mater. Exp. 1 (2) (2011) 278–292.

[15] R. Hübler, Transition metal nitrides thin films deposition using a dynamically controlled magnetron sputtering apparatus, Surf. Coat. Technol. 158–159 (2002) 680–684.

[16] L.R. Doolittle, Algorithms for the rapid simulation of Rutherford backscattering spectra, Nucl. Instrum. Methods Phys. Res., Sect. B 9 (3) (1985) 344–351.